HHS Public Access

Author manuscript

Neuroimage. Author manuscript; available in PMC 2020 October 01.

Published in final edited form as:

Neuroimage. 2019 October 01; 199: 184–193. doi:10.1016/j.neuroimage.2019.05.065.

Characterization of Lenticulostriate Arteries with High Resolution Black-blood T1-weighted Turbo Spin Echo with Variable Flip Angles at 3 and 7 Tesla

Samantha J. Ma[1], **Mona Sharifi Sarabi**[1], **Lirong Yan**[1], **Xingfeng Shao**[1], **Yue Chen**[2], **Qi Yang**[3], **Kay Jann**[1], **Arthur W Toga**[1], **Yonggang Shi**[1], **Danny J.J. Wang**[1,*]

[1]USC Stevens Neuroimaging and Informatics Institute, Department of Neurology, University of Southern California, Los Angeles, CA, USA

[2]Department of Radiology, Tianjin Renmin Hospital, Tianjin, China

[3]Department of Radiology, Xuanwu Hospital, Capital Medical University, Beijing, China

Abstract

Objectives—The lenticulostriate arteries (LSAs) with small diameters of a few hundred microns take origin directly from the high flow middle cerebral artery (MCA), making them especially susceptible to damage (e.g. by hypertension). This study aims to present high resolution (isotropic ~0.5 mm), black blood MRI for the visualization and characterization of LSAs at both 3T and 7T.

Materials and Methods—T1-weighted 3D turbo spin-echo with variable flip angles (T1w TSE-VFA) sequences were optimized for the visualization of LSAs by performing extended phase graph (EPG) simulations. Twenty healthy volunteers (15 under 35 years old, 5 over 60 years old) were imaged with the T1w TSE-VFA sequences at both 3T and 7T. Contrast-to-noise ratio (CNR) was quantified, and LSAs were manually segmented using ITK-SNAP. Automated Reeb graph shape analysis was performed to extract features including vessel length and tortuosity. All quantitative metrics were compared between the two field strengths and two age groups using ANOVA.

Results—LSAs can be clearly delineated using optimized 3D T1w TSE-VFA at 3T and 7T, and a greater number of LSA branches can be detected compared to those by time-of-flight MR angiography (TOF MRA) at 7T. The CNR of LSAs was comparable between 7T and 3T. T1w TSE-VFA showed significantly higher CNR than TOF MRA at the stem portion of the LSAs branching off the medial middle cerebral artery. The mean vessel length and tortuosity were greater on TOF MRA compared to TSE-VFA. The number of detected LSAs by both TSE-VFA and TOF MRA was significantly reduced in aged subjects, while the mean vessel length measured on 7T TSE-VFA showed significant difference between the two age groups.

[*]Corresponding to: Danny JJ Wang, PhD, MSCE, Laboratory of FMRI Technology (LOFT), Mark & Mary Stevens Neuroimaging and Informatics Institute, University of Southern California (USC), 2025 Zonal Avenue, Los Angeles, CA 90033, jwang71@gmail.com.

Conclusion—The high-resolution black-blood 3D T1w TSE-VFA sequence offers a new method for the visualization and quantification of LSAs at both 3T and 7T, which may be applied for a number of pathological conditions related to the damage of LSAs.

Keywords

lenticulostriate artery (LSA); Black blood MRI; Turbo spin echo with variable flip angles (TSE VFA); Subcortical vascular dementia; Ultrahigh magnetic field; 7T

1. Introduction

Small arteries and arterioles, particularly the lenticulostriate arteries (LSAs) are known to be involved in silent strokes, which contribute to progressive cognitive impairment in elderly persons. Detailed anatomical studies on the LSAs have been performed following the discovery of miliary aneurysms or microaneurysms along the LSAs by Charcot and Bouchard (Charcot and Bouchard, 1868). These studies revealed that the LSAs take origin directly from the high flow middle cerebral artery (MCA) and consist of either single vessels with small outer diameters of only 0.08–1.4 mm (Marinković et al., 2001) or branches off common stems with outer diameters of 0.6–1.8 mm (Umansky et al., 1985). This abrupt size and flow change makes them especially susceptible to damage (e.g. by hypertension) (Dichgans and Leys, 2017). The LSAs supply important subcortical areas including the caudate nucleus, globus pallidus, putamen, and part of the posterior limb of the internal capsule (Alexander, 1942; Beevor, 1907; Duret, 1873), and can be divided into medial and lateral groups. The lateral group commonly includes a LSA that Charcot called “the artery of the cerebral hemorrhage” which may rupture and result in an intracerebral hemorrhage and subsequent damage to the subcortical regions (Charcot, 1883). Additionally, LSAs are “end arteries”, meaning that the regions they supply have little or no collateral blood supply. When occluded, it produces a lacunar infarct in the tissue they supply. The origin of LSAs is also a common site of MCA aneurysm (Umansky et al., 1985).

High resolution time-of-flight MR angiography (TOF MRA) at ultrahigh magnetic field of 7T has been applied for the visualization of LSAs (Cho et al., 2008; Hendrikse et al., 2008). The morphology of these LSAs (e.g. branch number, radius, tortuosity) showed significant differences between subjects with subcortical vascular dementia (SVaD) and healthy controls (Seo et al., 2012) as well as between hypertensive and normotensive subjects (Kang et al., 2009b). These data demonstrate the potential for quantifying the morphology of LSAs as imaging biomarkers of hypertensive small vessel disease, which primarily affects subcortical regions. However, ultrahigh magnetic field is not commonly available in clinical practice. High-resolution black blood MRI is a technique originally developed for imaging intracranial vessel wall and plaques using 3D turbo spin-echo (TSE) sequences. Recently, TSE sequences (Alexander et al., 1998; Melhem et al., 1997) with variable flip angles (VFA) have been developed for black blood angiography (Yoneyama et al., 2012) and vessel wall imaging (Fan et al., 2016; Qiao et al., 2011; Qiao et al., 2014; van der Kolk et al., 2011). The long echo train of the TSE technique offers two advantages for visualizing small vessels: 1) adequate flow suppression by inherent dephasing of flowing signals (black blood MRI); 2) high spatial resolution (isotropic 0.5–0.6mm) and near whole-brain coverage in a clinically

acceptable time (<10min). These features suggest that TSE-VFA may also be suitable for imaging cerebral small vessels such as LSAs and other perforating arteries.

The purpose of this study was to present high resolution (isotropic ~0.5mm) 3D T1weighted TSE-VFA as a new approach for visualizing LSAs of young and aged subjects at standard clinical magnetic field strength of 3 Tesla and ultrahigh magnetic field of 7 Tesla. The imaging parameters of T1w TSE-VFA sequences were optimized through extended phase graph (EPG) simulations, and the visualization of LSAs was compared with that by TOF MRA at 7T. Quantitative metrics of LSA morphology were further derived by Reeb graph analysis of segmented LSA shapes which were compared between the two age groups and two field strengths, respectively. Unlike previous morphology analyses of LSAs that used two dimensional maximum intensity projections from TOF MRA at 7T (Kang et al., 2009a) or two dimensional minimum intensity projections from TSE-VFA at 3T (Zhang et al., 2019), we implemented a novel three-dimensional shape analysis of LSAs derived from T1-weighted TSE-VFA black-blood images to quantify the morphology of the vessels.

2. Methods

2.1 Extended Phase Graph Simulation

High-resolution black blood MRI with 3D TSE-VFA has been introduced recently for imaging intracranial vessel wall and plaques by utilizing an optimal VFA scheme to achieve a longer echo train length (ETL) for more effective flow suppression and a higher signal-to-noise ratio (SNR) efficiency compared to standard 3D TSE sequences (Busse et al., 2008; Mugler, 2014; Park et al., 2007; Qiao et al., 2011). However, existing 3D TSE-VFA techniques for vessel wall imaging were targeted for the suppression of relatively fast blood flow in large vessels as well as for maximizing the contrast between vessel wall and the surrounding cerebrospinal fluid (CSF). In order to enhance the visualization of small vessels such as LSAs and optimize the contrast between LSAs and surrounding brain tissue (white matter and deep gray matter), the spin evolutions of 3D T1w TSE-VFA were simulated using the EPG. In this study, we employed the default VFA scheme provided by the vendor for generating T1w contrast for black blood MRI (Fig. 1A)(Zhu et al., 2016). The signal evolution curves, or the magnetization transfer function (MTF), for various ETLs were generated using EPG simulation software (Hargreaves, 2012) developed in MATLAB (Mathworks, MA, USA) (Fig. 1B). The simulation considered the effects of the flip angles (FA) of the radiofrequency (RF) pulses, T1/T2 relaxations, and flow velocities on echo intensities (or the transverse magnetization component that develops during free precession). Point spread function (PSF) analysis was performed to evaluate the image blurring at higher field strength (Fig. 1C, top) or with a longer echo train (Fig. 1C, bottom), taking into account the elliptical-centric k-space ordering within the ky-kz plane (Busse et al., 2008) (see Supplemental Fig. S2B). The Fourier transform of the MTF is the PSF along the phase encode direction, and the full width at half maximum (FWHM) measurement can be used as a proxy for the effective resolution achieved in the image. Literature values of T1 and T2 relaxation times were used: T1/T2=1084/69 ms and T1/T2=1220/47 ms for white matter (WM) at 3T and 7T, respectively; T1/T2=1332/99 ms and T1/T2=1644/47 ms for deep gray matter (GM) at 3T and 7T, respectively; T1/T2=1932/275 ms and T1/T2=2587/68 ms for

arterial blood at 3T and 7T, respectively (Blockley et al., 2008; Cox, 2008; Dobre et al., 2007; Krishnamurthy et al., 2014; Li et al., 2016; Stanisz et al., 2005; Wright et al., 2008). As the LSAs are located among the white matter and deep gray matter, EPG simulations were performed for both tissues to achieve optimal results.

Using the EPG algorithm, we can observe the magnetization evolution and echo formation along multiple RF pulses. In order to incorporate slow flow dephasing of arterial blood signal within the LSAs into the EPG simulation, the following equation was used to calculate the accrued interpulse phase of the transverse magnetization, $\Delta\varphi(n)$:

$$\Delta\varphi\,(n) = \gamma\,\overrightarrow{v}\int_{(n-1)\tau}^{n\tau}\overrightarrow{G}\,(t)t\,dt \quad [1]$$

where γ is the gyromagnetic ratio (42.58 MHz/T), v is the average velocity of blood flow in small arteries (i.e. 4.5–8.2 cm/s) (Bouvy et al., 2016; Schnerr et al., 2017), n is the sequential order along the echo train, τ is half of the echo spacing, and G is the applied gradient amplitude. Laminar flow was employed to approximate the flow distribution in LSAs (Guyton and Hall, 1991). The flow distribution $p(v)$, or the area of the blood vessel cross-section containing blood traveling at velocities between v and $v+dv$ is given by (Maccotta et al., 1997)

$$p(v) = 1/v_{max} \quad [2]$$

where v_{max} is the maximum flow velocity. It can be shown that Eq. [1] still applies to laminar flow, with v being the average velocity of blood flow or half of v_{max} (see supplement for derivation). Based on the reported mean flow velocities in LSAs (4.5–8.2 cm/s) (Bouvy et al., 2016; Schnerr et al., 2017) and the first gradient moment (M1), the accrued interpulse phase can be estimated. In this experiment, the first gradient moments for the echo train along the 3 axes were: $M1_{readout}$ = 0.0936 mT·s2/m, $M1_{phase\text{-}encode}$ = 0.0225 mT·s2/m, $M1_{slice}$ = −6.8754 mT·s2/m at 3T; and $M1_{readout}$ = 0.0917 mT·s2/m, $M1_{phase\text{-}encode}$ = 0.0213 mT·s2/m, $M1_{slice}$ = −6.3806 mT·s2/m at 7T respectively. The gradient amplitude along the phase-encode (A-P) direction was used in the simulation to represent the most conservative estimate of flow induced phase accrual.

The calculated accrued phase term was added to the phase of each configuration state of the spin system associated with a refocusing RF pulse in the TSE sequence, as described previously (Weigel, 2015). As employed for *in vivo* scanning, the elliptical-centric ordering scheme was used for k-space encoding and the second echo was used as the TE. Following the echo train, the magnetization was rotated to the negative z-axis by a +90° RF pulse along the y-axis, which consequently suppressed the CSF signal (Becker and Farrar, 1969; Fan et al., 2017; Melhem et al., 2001; Van Uijen and Den Boef, 1984). Since CSF still has remaining transverse magnetization at the end of the echo train due to its long T2, the +90° RF pulse tips the magnetization to the negative z-axis, causing CSF signal attenuation at the

beginning of the following RF pulse train. Although CSF signal attenuation is not typically desired for intracranial angiography, this additional +90° RF pulse along the y-axis was evaluated for its effects on the LSA contrast. The simulations were performed with varying TRs and ETLs to optimize the contrast between arterial blood in LSAs and surrounding WM and deep GM respectively. In addition, the effect of B1 variations on the contrast between LSAs and WM was evaluated by repeating EPG simulations with B1 variations between −20% and 20%.

2.2 Subjects

A total of 23 healthy volunteers were recruited for this study after they provided written informed consent following a protocol approved by the Institutional Review Board (IRB) of the University of Southern California. Of these volunteers, 3 were excluded due to failures to complete the study protocol. Within the remaining 20 volunteers, 3 subjects (3 male, age 23.7 ± 2.5 years) participated in the pilot study to optimize the T1w TSE-VFA sequence. The other 17 healthy volunteers participated in the evaluation study of the optimized T1w TSE-VFA, including 12 participants (7 male, 27 ± 3.5 years) between 19–35 years of age and 5 participants (2 male, 64.2 ± 1.9 years) more than 60 years of age, herein referred to as the young and aged group, respectively. All participants were screened for history of or concurrent neurological or psychiatric disorder or systemic disease.

2.3 MRI Experiment

All MRI scans were performed on a Siemens 3T Prisma scanner with a product 32-channel head receive coil and body transmit coil, and on a Siemens 7T Terra scanner (Erlangen, Germany) with a single-channel transmit/32-channel receive (1Tx/32Rx) head coil (Nova Medical, Wilmington, MA, USA). The imaging protocols for T1w TSE-VFA were based on the clinical protocols of the SPACE (Sampling Perfection with Application optimized Contrast using different flip angle Evolution) sequence (Lichy et al., 2005) at 3 and 7T respectively. Pilot scans were performed at both 3T and 7T to evaluate the parameter optimization of TR and ETL (number of echoes) based on the EPG simulations. Additionally, various imaging parameters were evaluated including the use of slab-selective vs. non-selective excitation, saturation bands, magnetization restoration at the end of the echo train, and imaging slab orientation (sagittal vs. coronal). ECG triggering was also tested to evaluate the potential effect of flow pulsatility on the delineation of LSAs.

For the evaluation study, each participant underwent back-to-back scans on the 3T Prisma and 7T Terra systems, respectively, on the same day with counterbalanced order. The imaging protocol included a 3D MPRAGE structural scan at 3T (TR/TE=2300/2.98 ms, matrix=240×256, resolution=1×1×1 mm^3, scan time=5:12 min) and a 3D MP2RAGE structural scan at 7T (TR/TE=4500/3.43 ms, matrix = 320×320, resolution=0.7×0.7×0.7 mm^3, scan time=9:46 min). A high-resolution 3D time of flight (TOF) sequence for bright blood MR angiography (MRA) was performed at 7T for the visualization of the LSAs according to Kang et al. (TR/TE=12/4.67 ms, matrix=548×672, resolution=0.3×0.3×0.3 mm^3, GRAPPA factor = 3 in the phase-encode direction, FA = 20°, scan time=9:25 min) (Cho et al., 2008; Kang et al., 2009a). The optimized imaging protocols for T1w TSE-VFA were performed at 3T and 7T, respectively. Imaging parameters for 3T T1w TSE-VFA were:

TR/TE=1000/12 ms, turbo factor = 44, matrix size=756×896, resolution=0.51×0.51×0.64 mm^3, sagittal slab with 160 slices and 10% oversampling, GRAPPA factor = 2 in the phase-encode direction, total imaging time =8:39 min, 2 sagittal saturation bands were placed at the left and right temporal regions to suppress the out-of-FOV signals. Imaging parameters for 7T T1w TSE-VFA were: TR/TE=1200/13 ms, turbo factor = 40, matrix size= 320×320, resolution=0.5 mm^3 isotropic, sagittal slab with 288 slices and no slice oversampling, GRAPPA factor = 3 in the phase-encode direction, total imaging time =10:05 min. No saturation bands were applied due to specific absorption rate (SAR) limitations at 7T. For both 3T and 7T T1w TSE-VFA, an elliptical-centric ordering k-space sampling pattern (within ky-kz plane)(Busse et al., 2008) was employed to minimize potential head motion effects. Following the echo train, the magnetization was rotated to the negative z-axis by a +90° RF pulse along the y-axis to suppress the CSF signal (Fan et al., 2017; Van Uijen and Den Boef, 1984). The total time of the 3T and 7T study was typically 1.5 hours. The scan protocol parameters are summarized in Table 1.

To avoid degradation of the images due to motion, additional steps were implemented to physically limit motion including packing the head coil with cushions and applying paper tape across the coil on the forehead skin for tactile feedback.

2.4 Image Analysis

2.4.1 CNR quantification—All images were reviewed to ensure the absence of visible motion corruption or other artifacts. 3D T1w TSE-VFA images were reoriented in the coronal view, and LSAs were visualized by thin-slab (10 mm) minimum intensity projection (minIP) for qualitative review. The contrast to noise ratio (CNR) between arterial blood in the LSA and surrounding WM was calculated using Fiji software (Schindelin et al., 2012) by drawing a line across multiple dark vessels in an axial slice of the raw image data (such as the one shown in Figure 2) with slices containing the lateral stems, medial stems, lateral mid-length, and lateral distal portions, respectively. The signal intensity along the lines (i.e., signal profile in Figure 6 inset) was plotted. The signal intensities along the valleys (mean values in the lower quartile) were considered measures of the arterial blood signal. A 20 mm^2 circular region of interest (ROI) was drawn on the homogeneous WM that was adjacent to the basal ganglia region with matched locations on 3T and 7T images, respectively. The CNR was calculated by taking the signal intensity difference between WM and arterial blood of LSAs divided by the standard deviation of signals in the WM ROI (Zhang et al., 2019).

The raw images of TOF MRA at 7T were co-registered with 3D T1w TSE-VFA images at 7T in each subject using FreeSurfer (Fischl et al., 2002; Fischl et al., 2004) and Elastix version 4.8 (Klein et al., 2010; Shamonin et al., 2014) in Laboratory of Neuro Imaging (LONI) Pipeline (Rex et al., 2003). The CNR of TOF MRA was calculated along the same signal profile lines and WM ROI used for T1w TSE-VFA, except that the signal intensities along the peaks (mean values in the upper quartile) were taken as the arterial blood signal.

2.4.2 Vessel Segmentation and Morphology Metrics—We developed a three-step method to extract quantitative 3D measurements of LSAs for both TSE-VFA and TOF MRA

(Figure 2). As the first step, manual vessel segmentation was performed by an experienced neuroradiologist (Y.C.) using ITK-SNAP (Yushkevich et al., 2006). To increase the accuracy of vessel masks, raw images of all axial, coronal, and sagittal views were used in ITK-SNAP as shown in Figure 2a. However, geometric and topological outliers occur frequently during manual segmentation due to limited image resolution or anatomical variability across subjects. As the second step to perform quantitative shape analysis on these data, we applied the surface reconstruction method (Shi et al., 2010) that uses the Laplace-Beltrami (LB) spectrum for outlier removal without shrinkage (Figure 2b). The LB spectrum can be viewed as a generalization of the Fourier basis onto general surfaces. Building upon this intuitive understanding, the mesh reconstruction method (Shi et al., 2010) iteratively projects the mask boundary onto a subspace of low frequency LB eigenfunctions and removes outliers with large changes during the projection process. As shown in Figure 2, our method successfully obtains a smooth surface for each vessel (Figure 2b, vessel surface reconstruction). This fully automatic and iterative method allows the generation of a smooth surface representation of LSAs without shrinking other parts of the mask, and it ensures that all surfaces have a consistent genus-zero topology, which means all surfaces have no handle or hole in the reconstructed mesh (Xiao et al., 2003).

As the last step, the Reeb graph analysis method (Shi et al., 2008) was applied to model and extract geometrical measurements of 3D vessel shapes such as vessel length and tortuosity for 3T and 7T images, respectively (Figure 2c). The Reeb graph is an abstract graph describing the neighboring relation of the level contours of a function defined on a surface. Following our work on brain surfaces (Shi et al., 2013), we used the first non-constant LB eigenfunction as the feature function f for Reeb analysis. More specifically, we sampled 25 evenly spaced level contours of f as plotted on the vessel surface in Figure 2c. The centroid of each contour was used to explicitly represent the graph nodes. For the purpose of measuring the longest branch in each vessel, we assumed that the Reeb graph followed a chain topology, where each node on the graph only had up to two neighbors. To estimate the vessel length (Figure 2c), we extracted the center line or medial core of the 3D vessel surface by connecting the centroids of level contours, then summed up the distances of every two adjacent centroids. For vessel tortuosity, we used the common distance metric measure, which provides a ratio of the estimated vessel length to the Euclidean distance between the two end points of the curve. Vessel thickness could also be estimated; however, we chose not to report the results due to potential errors of small vessel size on the order of one voxel.

2.5 Statistical Analysis

Statistical analysis was performed with STATA 13.1 (College Station, Texas). CNR measurements were compared across the three techniques (T1w TSE-VFA at 3T and 7T, and TOF MRA at 7T) using within-subject ANOVA, followed by post-hoc paired t-test for pairwise comparison. Morphological metrics (vessel length, tortuosity) were subjected to Repeated-Measures ANOVA to evaluate the effect of age group, gender, field strength, and hemisphere. The total branch number was also compared across the three techniques (T1w TSE-VFA at 3T and 7T and TOF MRA at 7T) using within-subject ANOVA. A p-value $\leq$ 0.05 (two-sided) was considered statistically significant.

3. Results

3.1 EPG Simulations

The VFA schemes (Zhu et al., 2016) employed for T1w TSE are displayed in Figure 1A. The signal evolution along an echo train as well as the corresponding point-spread functions (PSF) taking into account the elliptical-centric k-space ordering (within the ky-kz plane, Supplemental Figure S2B) (Busse et al., 2008) are displayed in Figure 1B and 1C, respectively, for 3T (Figure 1, top row) and 7T (Figure 1, bottom row). Using the T1w VFA schemes provided by the vendor, the PSF was sharper at 7T (FWHM= 1.47 pixels) compared to 3T (FWHM=1.59 pixels). The employed VFA schemes also resulted in reduced T2 blurring along the echo train or sharper PSFs for longer ETLs at both 3 and 7T (Fig. 1C).

Taking into account phase accrual due to various blood flow velocities in the LSAs (4.5–8.2 cm/s), the optimal CNR between arterial blood and white matter was achieved with a TR of 1000 ms for the ETL of 33 and 41 or a TR of 1100 ms for the ETL of 60 at 3T, and a TR of 1200 ms for the ETL of 33, 41, and 60 at 7T, respectively (Figure 3A&B). The simulated CNR curves between arterial blood and deep gray matter at 3 and 7T respectively are shown in Figure 3C&D. The optimal CNR between arterial blood and deep gray matter was achieved with a TR of 1200 ms for the ETL of 33 and 41 or a TR of 1300 ms for the ETL of 60 at 3T, and a TR of 1300 ms for all 3 tested ETLs at 7T. Based on the simulation results to achieve the maximal CNR with an imaging time of 10min, the ETL of 40 with TR of 1000 ms and the ETL of 44 with TR of 1200 ms were employed for in vivo imaging at 3T and 7T, respectively (Figure 4). The effect of B1 variations on the contrast between LSAs and WM was also simulated, and the results showed that the contrast varied approximately linearly with the magnitude of B1 field, and the B1 effect was larger at 7T compared to 3T (Supplementary Figure S1).

3.2 Optimization of T1w TSE-VFA

Pilot studies were performed to optimize the T1w TSE-VFA protocol based on simulation results. Figure 4 shows a comparison of thin-slab (10 mm) minIP images of LSAs displayed with the same window/level settings using various imaging protocols (TR=600 or 1000 ms and ETL=40 or 60 at 3T; TR = 1200 ms and ETL = 44 or 60 at 7T). The experimental result matched well with EPG simulation results of Figure 3, resulting in the optimal TR of 1000 ms and ETL of 40 at 3T, and the optimal TR of 1200 ms and ETL of 44 at 7T. Improved sharpness of LSAs with the optimized T1w TSE-VFA protocol can be clearly seen. The +90°y pulse at the end of the echo train was evaluated for the effects on CNR. As shown in Supplementary Figure S3, the +90°y pulse further suppressed the CSF signal in the distal portions of the LSAs. However, the improved CNR between the LSAs and surrounding tissue enabled improved manual segmentation. The effect of ECG triggering is shown in Supplementary Figure S4 of minIP images of LSAs acquired without and with ECG triggering, respectively. Improved delineation of LSAs especially the distal branches can be seen with ECG triggering at the price of increased scan time (10–12 minutes depending on the cardiac rate). Sagittal and coronal slab orientations were compared and the results are shown in Supplementary Figure S5 with the table of sequence parameters in Supplemental Table 1. Coronal slab orientation had the potential advantage of more efficient coverage of

LSAs and reduced imaging time (7min 31sec); however, LSAs branching off the medial MCA were often missed compared to those observed using sagittal slab orientation, probably due to reduced SNR. Therefore, our final imaging protocol utilized sagittal slab orientation with TR=1000 ms/ETL=44 and TR=1200 ms/ETL=40 at 3T and 7T, respectively. ECG triggering was ultimately not employed due to prolonged scan time and potential variation in LSA contrast due to individual differences in cardiac rate.

3.3 Evaluation of T1w TSE-VFA

Figure 5 shows thin slab minIP images of LSAs from two representative young and two aged subjects using T1w TSE-VFA at 3T and 7T, as well as corresponding maximum intensity projection (MIP) images using TOF MRA at 7T. Qualitatively, LSAs were more clearly delineated with increased field strength, particularly in the distal portions of the vessels. T1w VFA-TSE at both 3T and 7T were able to resolve more LSAs than 7T TOF MRA ($p<0.05$), especially the LSAs located in the medial portion of the MCA (Figure 5, white arrows). As summarized in the bar plot of Figure 6, the CNR between LSAs and surrounding tissue were comparable between images acquired at 7T versus 3T for mid-length and distal portions of the LSAs. Compared to TOF MRA at 7T, the CNR of the stems of the LSAs originating from the lateral portion of the MCA in young subjects was significantly lower using T1w TSE-VFA (3T, $p=0.045$; 7T, $p = 0.034$). However, the CNR of the stems of the LSAs originating from the medial portion of the MCA in both young and aged subjects was significantly higher using T1w TSE-VFA compared to 7T TOF MRA (young 3T, $p= 0.001$; young 7T, $p=0.001$; aged 3T, $p=0.003$; aged 7T, $p<0.001$).

Figure 7 shows 3D renderings of manually segmented left LSAs on T1w TSE-VFA images at both 3T and 7T. Each primary vessel was assigned a different color label, with shorter secondary branches being given separate labels from the primary vessel. The total bilateral number of primary vessels counted using T1w TSE-VFA at 3T (mean ± SD: 11.00 ± 3.02) and 7T (11.65 ± 2.55) was significantly higher than that by TOF MRA at 7T (6.47 ± 1.68, $p=0.0001$). Additionally, significantly more secondary branches could be detected in 7T T1w TSE-VFA (3.75 ± 1.60, $p=0.0075$) compared to that at 3T (2.25 ± 1.71). Supplemental Figure S6 shows a few more examples of the 3D renderings where more branching was detected with 7T imaging. Metrics of vessel morphology including vessel length and tortuosity were quantified by Reeb graph analyses and subjected to ANOVA (see Table 2 for mean ± SD values of the metrics at 3T and 7T in two age groups, respectively). The effect of hemisphere and gender were not significant for both metrics. The effect of age group was significant for mean vessel length ($p=0.0257$), which was reduced in aged subjects for 7T TSE-VFA. The mean tortuosity was increased in aged subjects but the effect was not significant ($p=0.25$ for 7T TOF), as shown in the boxplots in Figure 8.

4. Discussion

4.1 Clinical Value of LSA Imaging

In this study, we presented high resolution (isotropic ~0.5mm), black blood T1w TSE-VFA for the visualization and characterization of LSAs at both 3 and 7T. To date, very few techniques are available for in vivo imaging of LSAs. Digital subtraction angiography

(DSA) and X-ray computed tomography angiography (CTA) have been applied for the characterization of LSAs in clinical populations (Gotoh et al., 2012; Kammerer et al., 2017). However, DSA is an invasive procedure and both DSA and CTA involve radiation exposure, precluding their use in healthy and/or preclinical populations. The sensitivity of DSA and CTA for visualizing LSAs is moderate with reported number of LSAs in the range of 1–7 (Gotoh et al., 2012). In contrast, the presented black blood MRI with T1w TSE-VFA is not only noninvasive, but also more sensitive in delineating LSAs with detected number of vessels (6–18) consistent with textbook descriptions of LSAs (Marinković et al., 2001; Umansky et al., 1985). Our technique may be useful for the clinical diagnosis of subcortical lacunar stroke and hemorrhages, and may be applied as a screening tool for LSA (micro)aneurysms in healthy populations.

4.2 T1w TSE VFA and 7T TOF MRA

TOF MRA at 7T has been proposed for visualizing and quantifying LSAs, which was considered impractical at lower field strengths (Cho et al., 2008). In this study, we presented optimized imaging protocols of T1w TSE-VFA at both 3T and 7T for visualizing LSAs. Compared to the reference standard of 7T TOF MRA, T1w TSE-VFA at both 3T and 7T were able to detect more primary stems of LSAs, although 7T TOF MRA enabled longer segmentation of the few LSAs that were detected. The CNR of 7T TOF MRA was greater than that of T1w TSE-VFA in relatively thick LSAs, however the saturation effect of TOF MRA on slow flowing spins led to compromised delineation of smaller LSAs. In contrast, our EPG simulation showed that small arteries with flow velocity in the range of 4.5–8.2 cm/s (Bouvy et al., 2016; Schnerr et al., 2017) can be reliably visualized by T1w TSE-VFA due to combined effects of longer T1/T2 values of arterial blood and flow induced phase dispersion during TSE readout at both 3T and 7T. These simulation results were further verified by in vivo experimental data, suggesting T1w TSE-VFA may outperform 7T TOF MRA for visualizing (small) medial LSAs at both clinical field strength and ultrahigh magnetic field. Black blood MRI also allows simultaneous assessment of vessel wall and parenchymal lesions. It is worth noting that the TOF MRA protocol in our experiment was not as fully optimized as that of TSE-VFA, so the comparison results between the two techniques may need to be interpreted with caution.

For black blood MRI with T1w TSE-VFA, the CNR of LSAs was comparable at 3T with that at 7T, although significantly more LSA secondary branches could be delineated at 7T. The spatial resolution of T1w TSE-VFA was slightly lower at 3T (voxel size = $0.51\times0.51\times0.64mm^3$) than 7T ($0.5\times0.5\times0.5mm^3$) in the present study. The reduced T2 blurring and sharper PSF at 7T enabled easier identification of LSAs, and the segmented vessel lengths were significantly longer than that at 3T. However, the other LSA metrics including vessel number and tortuosity, were not significantly different between 3T and 7T, suggesting 3T T1w TSE-VFA may be sufficient for capturing the morphology of LSAs. It must be noted that the above metrics were derived from manual segmentation of LSAs, which is time consuming and may be subjective. For automated segmentation of LSAs, the sharpness and improved SNR at 7T may be more advantageous. In addition, the 7T Terra MR system used in the present study is the first FDA approved ultrahigh field MR system.

All developed MR pulse sequences and imaging protocol can therefore be directly translated to clinical imaging.

4.3 Aging Effects on LSAs

In the present study, significant differences between the two age groups were found for the number of detected LSAs. These results are consistent with recent findings of a reduced number of perforators in the basal ganglia of patients with lacunar infarction compared to matched controls (Geurts Lennart et al., 2019). There was also a trend of decreased mean vessel length and increased mean tortuosity in the aged group. A recent phase-contrast (PC) MRI study assessed flow pulsatility of LSAs at 7T and found increased pulsatility index and reduced damping factor of LSA blood flow in aged subjects, suggesting increased stiffness and reduced vascular compliance of LSAs with aging (Schnerr et al., 2017). The reported mean (minimum–maximum) flow velocity was 8.2 (6.2–10.1) cm/s and 4.5 (2.9–6.1) cm/s in young and aged subjects, and the number of LSAs that can be reliably identified for flow measurement was 3–7 and 3–4 in young and aged subjects, respectively. Our data of reduced vessel number and length in aged subjects are highly consistent with the PC MRI study, suggesting that reduced flow velocity and pulsatility index may contribute to impaired visualization of LSAs in T1w TSE-VFA scans.

Our data is also consistent with past studies quantifying the morphology of LSAs showing significant differences between subjects with subcortical vascular dementia (SVaD) and healthy controls (Seo et al., 2012) as well as between hypertensive and normotensive subjects (Kang et al., 2009b). With the presence of vascular risk factors such as diabetes, hypertension, and hyperlipidemia, the LSA metrics such as vessel number and length may further decrease compared to healthy controls. However, increased LSA tortuosity has been reported in vascular dementia compared to age matched controls (Seo et al., 2012). While this trend of increased tortuosity of LSAs in aged subjects was observed in the 7T TOF scans of our study, there was no significant difference in tortuosity when evaluated using TSE-VFA images at 3 or 7T. As the morphologic metrics in our study were derived from manually segmented LSAs, it is possible that the distal portions of LSAs were not well-detected by the human eye. As a result, tortuosity was mainly quantified in larger LSA stems, leading to similar tortuosity in aged subjects (tortuosity is defined as the ratio between the actual path length divided by the linear distance). It is also possible that tortuosity of LSAs may increase and subsequently contribute to altered blood brain barrier permeability at the distal ends of these perforators in aged subjects at risk of developing cerebral small vessel disease and dementia compared to age matched controls (Shao et al., 2019). This hypothesis is being tested in our lab on a cohort of aged subjects.

Due to the relatively long acquisition time, a limitation of the black blood MRI sequence is the possibility for motion, especially in the less compliant aged subjects. Motion artifacts such as blurring and ghosting were observed in the TSE-VFA images of the excluded subjects who failed to complete the MRI scans. Motion artifacts can also affect the manual segmentation in aged subjects, since even a slight shift of the head can affect the visualization of the 80–1400 μm diameter LSAs. Due to the use of packing in the head coil

and applying paper tape across the forehead skin for tactile feedback, the black blood MRI data included in our analyses were free of visible motion or other artifacts.

4.4 LSA Segmentation and Shape Quantification

Using manual segmentation and automated surface modeling, we performed fully 3D analyses of the LSA morphometry in this study. The vessel counts observed for each modality using manual segmentation in this study align with the findings of number of stems (two to ten) and tortuosity observed in previous 7T TOF studies (Kang et al., 2009a; Kang et al., 2009b; Seo et al., 2012). The surface reconstruction and Reeb graph analysis methods provided a consistent representation for the comparison of vessel geometry across subjects and vessel branches. Significant differences were detected between age groups based on the measures from Reeb graph modeling. While we used manually delineated masks for our quantification, the 3D shape analysis tools can be directly applied to automated segmentation results when they become available. This will be a main direction for our future research. The manually segmented masks form a reasonable training data for supervised learning algorithms if we consider that there are typically 10+ vessel branches from each subject. For medical image segmentation, patch-based deep learning segmentation algorithms have achieved success in various tasks (Kamnitsas et al., 2017; Wachinger et al., 2018). We will leverage these frameworks for our research on automated LSA segmentation as they fit very well with the vessel segmentation problem, which is inherently based on contrasts in a local neighborhood.

4.5 Limitations of the Study

There are several limitations of this study. First, T1w TSE-VFA also suppresses CSF due to its long T1/T2 values; therefore, the delineated LSAs may include perivascular space (PVS). However, we have compared T1w TSE-VFA and T2w TSE-VFA (Supplementary Figure S7), which delineates PVS; and the locations of LSAs in black blood MRI did not completely match those of PVS in the basal ganglia area. Another possibility is to combine complementary flow suppression techniques like DANTE (Viessmann et al., 2017; Xie et al., 2016) with the T1w VFA-TSE sequence to further suppress the signal of moving spins in arterial blood and improve black-blood contrast. Second, the image contrast of LSAs may be affected by B1 inhomogeneity, especially at 7T. Nevertheless, the central location of LSAs at the “bright spot” of B1+ field due to dielectric effects at 7T is favorable for enhancing the CNR of LSAs, based on our simulation (Supplemental Figure S1). The region of interest for estimating the noise was taken from a relatively uniform white matter region within this “bright spot”, although the number of voxels in this region may not be as large as ideally required for the estimation of the standard deviation (Greenwood and Sandomire, 1950; Kellman and McVeigh, 2005). Third, the scan time of T1w TSE-VFA was relatively long (8:39 min at 3T and 10:05 min at 7T) making black blood MRI susceptible to motion artifacts. In order to reduce scan time, we have attempted zoomed TSE (Ma et al., 2017) and accelerated TSE with 2D CAIPI acquisition (Fritz et al., 2016). However, these two techniques caused reduced SNR and CNR, hindering the delineation of LSAs. In the future, prospective motion correction techniques using optical and/or RF tracking (Callaghan et al., 2015) may be applied in conjunction with sparse sampling techniques such as compressed sensing. Due to SAR limitations at 7T, the imaging protocols and resolutions of TSE-VFA

were not identical at 3 and 7T. However, they were developed based on the best clinical practice at each field strength. Finally, manual segmentation of LSAs is time consuming and subjective. We are developing machine learning algorithms to automatically segment LSAs and quantify their shapes, using the manually segmented LSAs as the model for training.

5. Conclusions

High-resolution black-blood 3D T1w TSE-VFA sequence offers a new method for the visualization and quantification of LSAs at both 3T and 7T, which may serve as a promising imaging marker of pathological conditions related to damaged LSAs.

Supplementary Material

Refer to Web version on PubMed Central for supplementary material.

ACKNOWLEDGEMENT

This work was supported by National Institute of Health (NIH) grants UH2-NS100614, S10-OD025312, K25-AG056594 and P41-EB015922. This work was also supported by American Heart Association (AHA) grant 16SDG29630013.

References

Alexander AL, Buswell HR, Sun Y, Chapman BE, Tsuruda JS, Parker DL, 1998 Intracranial black-blood MR angiography with high-resolution 3D fast spin echo. Magn Reson Med 40, 298–310. [PubMed: 9702712]

Alexander L, 1942 The vascular supply of the strio-palladium. Res Publ Assoc Res Nerv Ment Dis 21, 77–132.

Becker ED, Farrar TC, 1969 Driven equilibrium Fourier transform spectroscopy. A new method for nuclear magnetic resonance signal enhancement. J Am Chem Soc 91, 7784–7785. [PubMed: 5357869]

Beevor CE, 1907 The cerebral arterial supply. Brain 30, 403–425.

Blockley NP, Jiang L, Gardener AG, Ludman CN, Francis ST, Gowland PA, 2008 Field strength dependence of R1 and R 2* relaxivities of human whole blood to prohance, vasovist, and deoxyhemoglobin. Magnetic Resonance in Medicine 60, 1313–1320. [PubMed: 19030165]

Bouvy WH, Geurts LJ, Kuijf HJ, Luijten PR, Kappelle LJ, Biessels GJ, Zwanenburg JJM, 2016 Assessment of blood flow velocity and pulsatility in cerebral perforating arteries with 7-<dummy_junk>T quantitative flow MRI. Nmr in Biomedicine 29, 1295–1304. [PubMed: 25916399]

Busse RF, Brau AC, Vu A, Michelich CR, Bayram E, Kijowski R, Reeder SB, Rowley HA, 2008 Effects of refocusing flip angle modulation and view ordering in 3D fast spin echo. Magn Reson Med 60, 640–649. [PubMed: 18727082]

Callaghan MF, Josephs O, Herbst M, Zaitsev M, Todd N, Weiskopf N, 2015 An evaluation of prospective motion correction (PMC) for high resolution quantitative MRI. Frontiers in Neuroscience 9, 97. [PubMed: 25859178]

Charcot J, Bouchard C, 1868 Nouvelles recherches sur la pathogenie de l'hemorrhagie cerebrale. Arch Physiol Norm Pathol 1, 110–127, 643–665.

Charcot JM, 1883 Lectures VII, VIII, and IX, in Hadden WB (ed): Lectures on Localization of Cerebral and Spinal Diseases. London: The New Sydenham Society, pp 46–97.

Cho ZH, Kang CK, Han JY, Kim SH, Kim KN, Hong SM, Park CW, Kim YB, 2008 Observation of the lenticulostriate arteries in the human brain in vivo using 7.0T MR angiography. Stroke 39, 1604–1606. [PubMed: 18340096]

Cox EF, Gowland PA, 2008 Measuring T2 and T2' in the brain at 1.5T, 3T and 7T using a hybrid gradient echo-spin echo sequence and EPI. Proc. Intl. Soc. Mag. Reson. Med, Toronto, Canada.

Dichgans M, Leys D, 2017 Vascular Cognitive Impairment. Circ Res 120, 573–591. [PubMed: 28154105]

Dobre MC, Uğurbil K, Marjanska M, 2007 Determination of blood longitudinal relaxation time (T1) at high magnetic field strengths. Magnetic Resonance Imaging 25, 733–735. [PubMed: 17540286]

Duret H, 1873 Note sur la circulation du corps strié. Progres Medical 1, 259–260.

Fan Z, Yang Q, Deng Z, Li Y, Bi X, Song S, Li D, 2016 Whole-brain intracranial vessel wall imaging at 3 Tesla using cerebrospinal fluid-attenuated T1-weighted 3D turbo spin echo. Magn Reson Med.

Fan Z, Yang Q, Deng Z, Li Y, Bi X, Song S, Li D, 2017 Whole-Brain Intracranial Vessel Wall Imaging at 3 Tesla Using Cerebrospinal Fluid–Attenuated T1-Weighted 3D Turbo Spin Echo. Magnetic Resonance in Medicine 77, 1142–1150. [PubMed: 26923198]

Fischl B, Salat DH, Busa E, Albert M, Dieterich M, Haselgrove C, van der Kouwe A, Killiany R, Kennedy D, Klaveness S, Montillo A, Makris N, Rosen B, Dale AM, 2002 Whole brain segmentation: automated labeling of neuroanatomical structures in the human brain. Neuron 33, 341–355. [PubMed: 11832223]

Fischl B, Salat DH, van der Kouwe AJ, Makris N, Segonne F, Quinn BT, Dale AM, 2004 Sequence-independent segmentation of magnetic resonance images. NeuroImage 23 Suppl 1, S69–84. [PubMed: 15501102]

Fritz J, Fritz B, Thawait GG, Meyer H, Gilson WD, Raithel E, 2016 Three-Dimensional CAIPIRINHA SPACE TSE for 5-Minute High-Resolution MRI of the Knee. Investigative Radiology 51, 609–617. [PubMed: 27187045]

Geurts Lennart J, Zwanenburg Jaco JM, Klijn Catharina JM, Luijten Peter R, Biessels Geert J, 2019 Higher Pulsatility in Cerebral Perforating Arteries in Patients With Small Vessel Disease Related Stroke, a 7T MRI Study. Stroke 50, 62–68.

Gotoh K, Okada T, Satogami N, Yakami M, Takahashi JC, Yoshida K, Ishii A, Tanaka S, Miyamoto S, Togashi K, 2012 Evaluation of CT angiography for visualisation of the lenticulostriate artery: difference between normotensive and hypertensive patients. The British Journal of Radiology 85, e1004–e1008. [PubMed: 22744324]

Greenwood JA, Sandomire MM, 1950 Sample Size Required for Estimating the Standard Deviation as a Per Cent of its True Value. Journal of the American Statistical Association 45, 257–260.

Guyton AC, Hall JE, 1991 Textbook of Medical Physiology. W. B. Saunders, Philadelphia.

Hargreaves B, 2012 EPG Lecture. Stanford University.

Hendrikse J, Zwanenburg JJ, Visser F, Takahara T, Luijten P, 2008 Noninvasive depiction of the lenticulostriate arteries with time-of-flight MR angiography at 7.0 T. Cerebrovasc Dis 26, 624–629. [PubMed: 18984947]

Kammerer S, Mueller-Eschner M, Berkefeld J, Tritt S, 2017 Time-resolved 3D Rotational Angiography (4D DSA) of the Lenticulostriate Arteries: Display of Normal Anatomic Variants and Collaterals in Cases with Chronic Obstruction of the MCA. Clin Neuroradiol 27, 451–457. [PubMed: 28352979]

Kamnitsas K, Ledig C, Newcombe VFJ, Simpson JP, Kane AD, Menon DK, Rueckert D, Glocker B, 2017 Efficient multi-scale 3D CNN with fully connected CRF for accurate brain lesion segmentation. Medical Image Analysis 36, 61–78. [PubMed: 27865153]

Kang C-K, Park C-W, Han J-Y, Kim S-H, Park C-A, Kim K-N, Hong S-M, Kim Y-B, Lee KH, Cho Z-H, 2009a Imaging and analysis of lenticulostriate arteries using 7.0-Tesla magnetic resonance angiography. Magnetic Resonance in Medicine 61, 136–144. [PubMed: 19097221]

Kang CK, Park CA, Lee H, Kim SH, Park CW, Kim YB, Cho ZH, 2009b Hypertension correlates with lenticulostriate arteries visualized by 7T magnetic resonance angiography. Hypertension 54, 1050–1056. [PubMed: 19805635]

Kellman P, McVeigh ER, 2005 Image reconstruction in SNR units: a general method for SNR measurement. Magn Reson Med 54, 1439–1447. [PubMed: 16261576]

Klein S, Staring M, Murphy K, Viergever MA, Pluim JPW, 2010 Elastix: A Toolbox for Intensity-Based Medical Image Registration. IEEE Transactions on Medical Imaging 29, 196–205. [PubMed: 19923044]

Krishnamurthy LC, Liu P, Xu F, Uh J, Dimitrov I, Lu H, 2014 Dependence of blood T2 on oxygenation at 7 T: In vitro calibration and in vivo application. Magnetic Resonance in Medicine 71, 2035–2042. [PubMed: 23843129]

Li W, Grgac K, Huang A, Yadav N, Qin Q, van Zijl Peter CM, 2016 Quantitative theory for the longitudinal relaxation time of blood water. Magnetic Resonance in Medicine 76, 270–281. [PubMed: 26285144]

Lichy MP, Wietek B, Mugler JP III, Horger W, Menzel M, Siegmann K, Martirosian P, Kiefer B, 2005 Whole-body applications of isotropic high-resolution T2-weighted MRI with a single slab 3D-TSE based sequence optimized for high sampling efficiency, called SPACE - initial clinical experiences. Miami Beach, Florida, USA, p. 794.

Ma SJ, Gahm JK, Yan L, Shen Y, Shao X, Shi Y, Wang DJJ, 2017 Evaluation of Whole Brain and ZOOMit T1-weighted Turbo-Spin Echo (TSE) for Visualization of Human Lenticulostriate Arteries at 3.0 T: A Preliminary Study. International Society of Magnetic Resonance in Medicine Annual Meeting, Honolulu, HI, USA, p. 2565.

Maccotta L, Detre JA, Alsop DC, 1997 The efficiency of adiabatic inversion for perfusion imaging by arterial spin labeling. NMR Biomed 10, 216–221. [PubMed: 9430351]

Marinković S, Gibo H, Milisavljević M, Ćetković M, 2001 Anatomic and clinical correlations of the lenticulostriate arteries. Clinical Anatomy 14, 190–195. [PubMed: 11301466]

Melhem ER, Itoh R, Folkers PJM, 2001 Cervical Spine: Three-dimensional Fast SpinEcho MR Imaging—Improved Recovery of Longitudinal Magnetization with Driven Equilibrium Pulse. Radiology 218, 283–288. [PubMed: 11152816]

Melhem ER, Jara H, Yucel EK, 1997 Black blood MR angiography using multislab three-dimensional TI-weighted turbo spin-echo technique: imaging of intracranial circulation. AJR Am J Roentgenol 169, 1418–1420. [PubMed: 9353471]

Mugler JP 3rd, 2014 Optimized three-dimensional fast-spin-echo MRI. J Magn Reson Imaging 39, 745–767. [PubMed: 24399498]

Park J, Mugler JP 3rd, Horger W, Kiefer B, 2007 Optimized T1-weighted contrast for single-slab 3D turbo spin-echo imaging with long echo trains: application to whole-brain imaging. Magn Reson Med 58, 982–992. [PubMed: 17969106]

Qiao Y, Steinman DA, Qin Q, Etesami M, Schar M, Astor BC, Wasserman BA, 2011 Intracranial arterial wall imaging using three-dimensional high isotropic resolution black blood MRI at 3.0 Tesla. J Magn Reson Imaging 34, 22–30. [PubMed: 21698704]

Qiao Y, Zeiler SR, Mirbagheri S, Leigh R, Urrutia V, Wityk R, Wasserman BA, 2014 Intracranial plaque enhancement in patients with cerebrovascular events on high-spatial-resolution MR images. Radiology 271, 534–542. [PubMed: 24475850]

Rex DE, Ma JQ, Toga AW, 2003 The LONI Pipeline Processing Environment. NeuroImage 19, 1033–1048. [PubMed: 12880830]

Schindelin J, Arganda-Carreras I, Frise E, Kaynig V, Longair M, Pietzsch T, Preibisch S, Rueden C, Saalfeld S, Schmid B, Tinevez J-Y, White DJ, Hartenstein V, Eliceiri K, Tomancak P, Cardona A, 2012 Fiji: an open-source platform for biological-image analysis. Nature Methods 9, 676. [PubMed: 22743772]

Schnerr RS, Jansen JFA, Uludag K, Hofman PAM, Wildberger JE, van Oostenbrugge RJ, Backes WH, 2017 Pulsatility of Lenticulostriate Arteries Assessed by 7 Tesla Flow MRI—Measurement, Reproducibility, and Applicability to Aging Effect. Frontiers in Physiology 8, 961. [PubMed: 29225580]

Seo SW, Kang CK, Kim SH, Yoon DS, Liao W, Worz S, Rohr K, Kim YB, Na DL, Cho ZH, 2012 Measurements of lenticulostriate arteries using 7T MRI: new imaging markers for subcortical vascular dementia. J Neurol Sci 322, 200–205. [PubMed: 22664155]

Shamonin D, Bron E, Lelieveldt B, Smits M, Klein S, Staring M, 2014 Fast Parallel Image Registration on CPU and GPU for Diagnostic Classification of Alzheimer's Disease. Frontiers in Neuroinformatics 7.

Shao X, Ma SJ, Casey M, D'Orazio L, Ringman JM, Wang DJJ, 2019 Mapping water exchange across the blood–brain barrier using 3D diffusion-prepared arterial spin labeled perfusion MRI. Magnetic Resonance in Medicine 81, 3065–3079. [PubMed: 30561821]

Shi Y, Lai R, Krishna S, Sicotte N, Dinov I, Toga AW, 2008 Anisotropic Laplace-Beltrami eigenmaps: Bridging Reeb graphs and skeletons. 2008 IEEE Computer Society Conference on Computer Vision and Pattern Recognition Workshops, pp. 1–7.

Shi Y, Lai R, Morra JH, Dinov I, Thompson PM, Toga AW, 2010 Robust Surface Reconstruction via Laplace-Beltrami Eigen-Projection and Boundary Deformation. IEEE Transactions on Medical Imaging 29, 2009–2022. [PubMed: 20624704]

Shi Y, Lai R, Toga AW, Alzheimer's Disease Neuroimaging I, 2013 Cortical surface reconstruction via unified Reeb analysis of geometric and topological outliers in magnetic resonance images. IEEE Trans Med Imaging 32, 511–530. [PubMed: 23086519]

Stanisz GJ, Odrobina EE, Pun J, Escaravage M, Graham SJ, Bronskill MJ, Henkelman RM, 2005 T1, T2 relaxation and magnetization transfer in tissue at 3T. Magnetic Resonance in Medicine 54, 507–512. [PubMed: 16086319]

Umansky F, Gomes FB, Dujovny M, Diaz FG, Ausman JI, Mirchandani HG, Berman SK, 1985 The perforating branches of the middle cerebral artery. Journal of Neurosurgery 62, 261–268. [PubMed: 3968566]

van der Kolk AG, Zwanenburg JJ, Brundel M, Biessels GJ, Visser F, Luijten PR, Hendrikse J, 2011 Intracranial vessel wall imaging at 7.0-T MRI. Stroke 42, 2478–2484. [PubMed: 21757674]

Van Uijen CMJ, Den Boef JH, 1984 Driven-equilibrium radiofrequency pulses in NMR imaging. Magnetic Resonance in Medicine 1, 502–507. [PubMed: 6571572]

Viessmann O, Li L, Benjamin P, Jezzard P, 2017 T2-Weighted intracranial vessel wall imaging at 7 Tesla using a DANTE-prepared variable flip angle turbo spin echo readout (DANTE-SPACE). Magn Reson Med 77, 655–663. [PubMed: 26890988]

Wachinger C, Reuter M, Klein T, 2018 DeepNAT: Deep convolutional neural network for segmenting neuroanatomy. Neuroimage 170, 434–445. [PubMed: 28223187]

Weigel M, 2015 Extended phase graphs: Dephasing, RF pulses, and echoes - pure and simple. Journal of Magnetic Resonance Imaging 41, 266–295. [PubMed: 24737382]

Wright PJ, Mougin OE, Totman JJ, Peters AM, Brookes MJ, Coxon R, Morris PE, Clemence M, Francis ST, Bowtell RW, Gowland PA, 2008 Water proton T 1 measurements in brain tissue at 7, 3, and 1.5T using IR-EPI, IR-TSE, and MPRAGE: results and optimization. Magnetic Resonance Materials in Physics, Biology and Medicine 21, 121.

Xiao H, Chenyang X, Prince JL, 2003 A topology preserving level set method for geometric deformable models. IEEE Transactions on Pattern Analysis and Machine Intelligence 25, 755–768.

Xie Y, Yang Q, Xie G, Pang J, Fan Z, Li D, 2016 Improved black-blood imaging using DANTE-SPACE for simultaneous carotid and intracranial vessel wall evaluation. Magnetic Resonance in Medicine 75, 2286–2294. [PubMed: 26152900]

Yoneyama M, Nakamura M, Tabuchi T, Takemura A, Obara M, 2012 Optimization of 3D-variable refocusing flip angle RARE imaging for high-resolution volumetric black-blood angiography. Radiol Phys Technol 5, 270–276. [PubMed: 22714282]

Yushkevich PA, Piven J, Hazlett HC, Smith RG, Ho S, Gee JC, Gerig G, 2006 Userguided 3D active contour segmentation of anatomical structures: Significantly improved efficiency and reliability. NeuroImage 31, 1116–1128. [PubMed: 16545965]

Zhang Z, Fan Z, Kong Q, Xiao J, Wu F, An J, Yang Q, Li D, Zhuo Y, 2019 Visualization of the lenticulostriate arteries at 3T using black-blood T1-weighted intracranial vessel wall imaging: comparison with 7T TOF-MRA. Eur Radiol 29, 1452–1459. [PubMed: 30151642]

Zhu C, Haraldsson H, Tian B, Meisel K, Ko N, Lawton M, Grinstead J, Ahn S, Laub G, Hess C, Saloner D, 2016 High resolution imaging of the intracranial vessel wall at 3 and 7 T using 3D fast spin echo MRI. Magma 29, 559–570. [PubMed: 26946509]

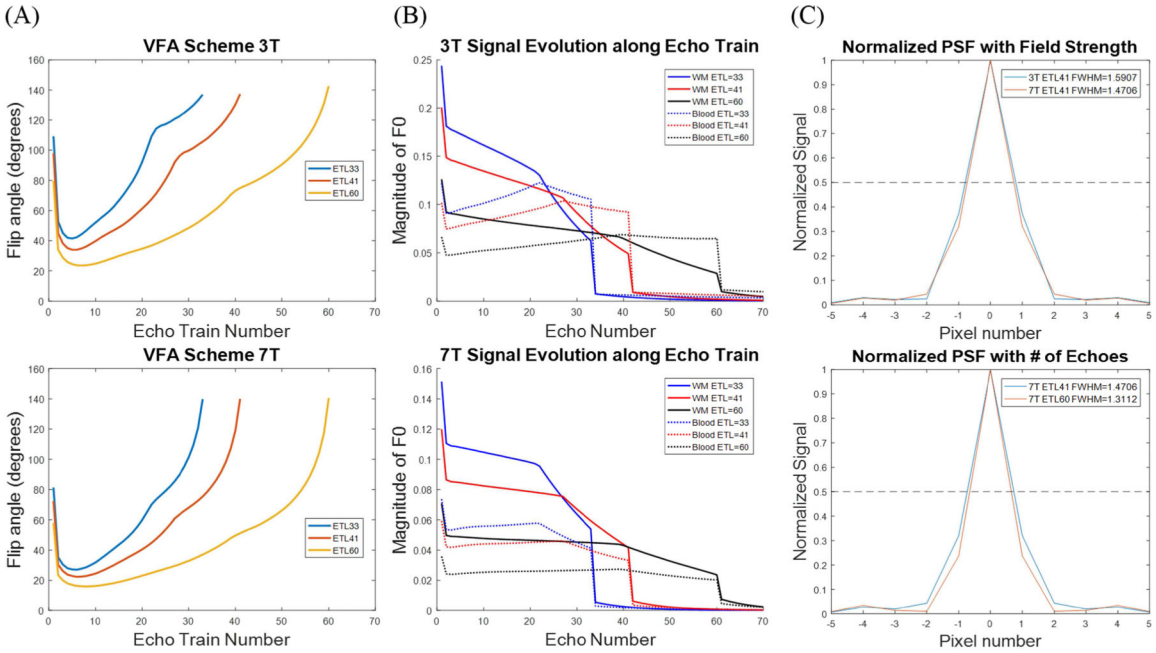

Figure 1.

The variable flip angle schemes from the 3T Siemens Prisma (A, top) and the 7T Siemens Terra (A, bottom) T1w TSE-VFA sequence. Signal evolution curves were created using extended phase graph simulations for 3T parameters (B, top) and 7T parameters (B, bottom). Normalized point spread functions along the phase encode direction were calculated by taking the Fourier transform of the magnetization transfer function (MTF, in B) to evaluate T2 blurring due to field strength (C, top) and echo train length (C, bottom).

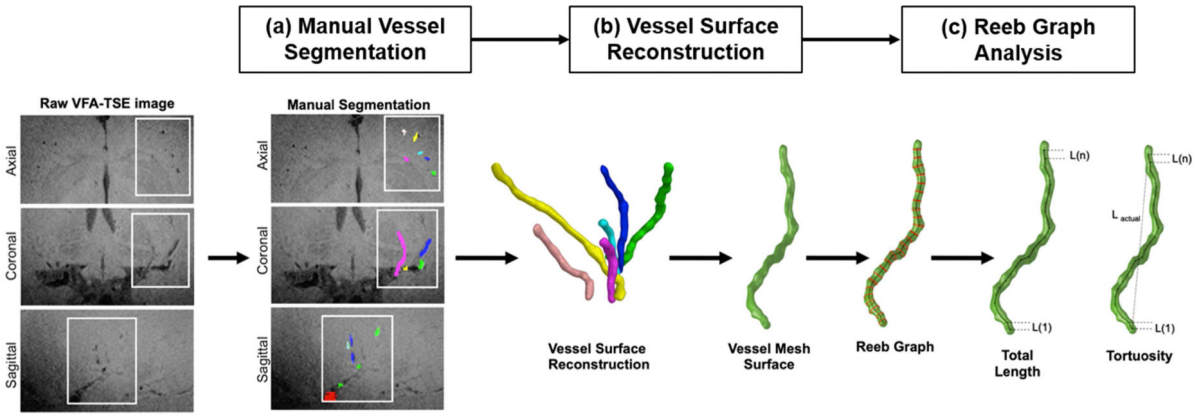

Figure 2.

Lenticulostriate artery morphological quantification workflow begins with manual vessel segmentation using ITK-SNAP on the raw TSE-VFA image (a). The vessel volumes are reconstructed, and a mesh surface is created in preparation for shape analysis (b). Quantitative measures such as vessel length and tortuosity are calculated from the Reeb graph (c).

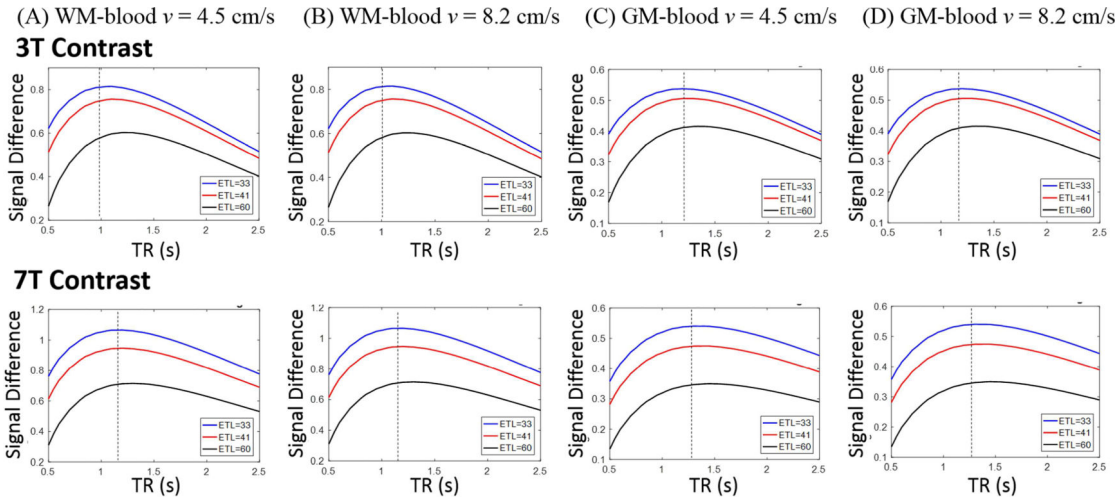

Figure 3.

Plots of the signal difference between arterial blood and either white matter (WM) or deep gray matter (GM) as a function of TR for 3 different echo train lengths (ETLs) and blood flow velocities (4.5 cm/s for aged (A, C), and 8.2 cm/s for young (B, D)) respectively. The optimal TR is 1000 ms for T1w TSE-VFA at 3T (top row) and 1200 ms at 7T (bottom row) for signal difference between WM and blood. The optimal TR is 1200 ms for T1w TSE-VFA at 3T and 1300 ms at 7T for signal difference between deep GM and blood (dashed lines).

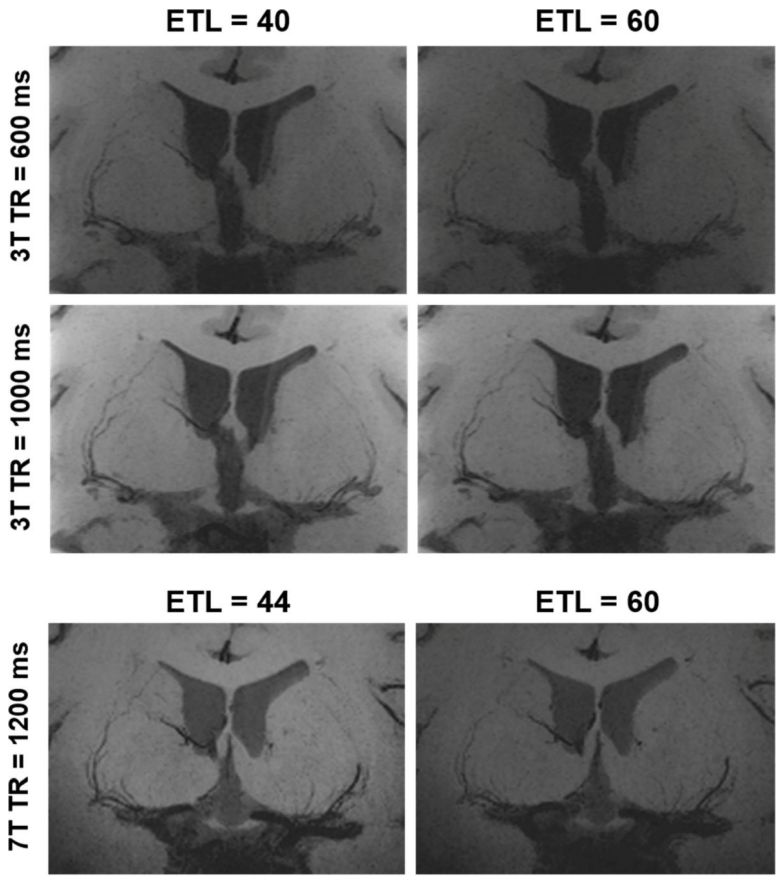

Figure 4.

Coronal 10 mm thin slice minimum intensity projections of pilot scans using echo train length (ETL) of 40 or 60, and TR of 600 ms and 1000 ms at 3T (top two rows), and TR of 1200 ms at 7T (bottom row), set to the same window level. The pilot scan results confirm trends observed in the EPG simulation, in which the best contrast is observed for ETL = 40 and TR = 1000 ms at 3T. Due to SAR limitations for short TR at 7T, the theoretical optimal TR of 1200 ms was used, and the contrast observed with ETL = 44 is better than that of ETL = 60.

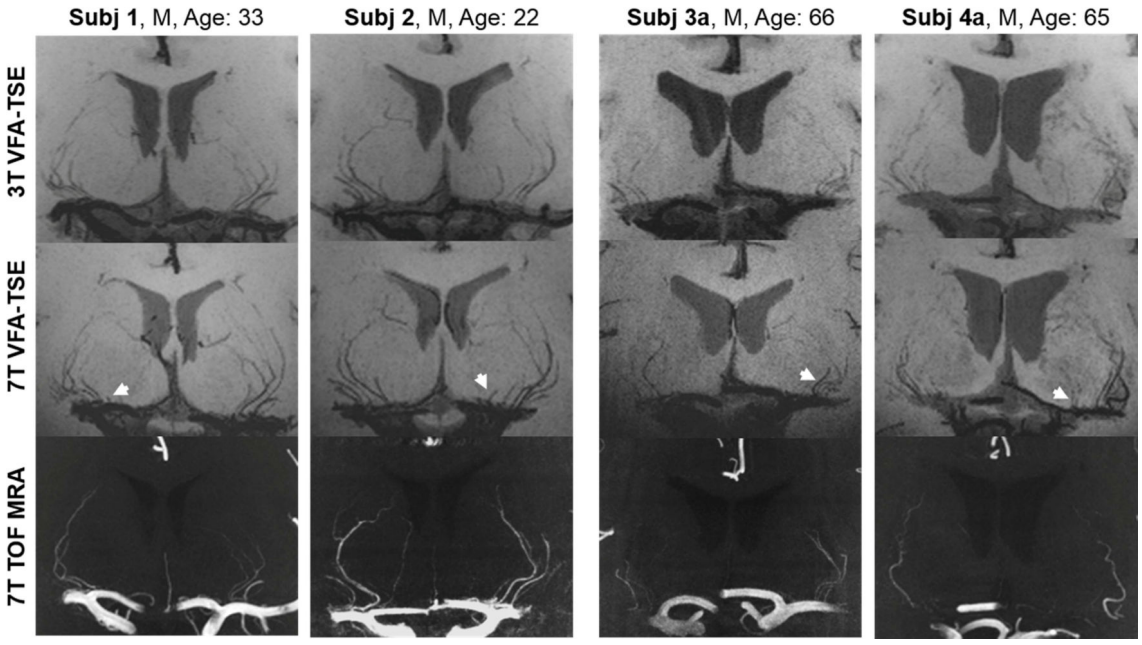

Figure 5.

Coronal 10 mm thin slice minimum intensity projections of both young and aged subject TSE-VFA scans at 3.0 Tesla (top row) and 7.0 Tesla (middle row). The bottom row shows coronal 10 mm thin slice maximum intensity projection of 7T TOF MRA. TSE-VFA can resolve more LSAs than 7T TOF MRA, especially for the LSAs located in the medial group along the middle cerebral artery (white arrows).

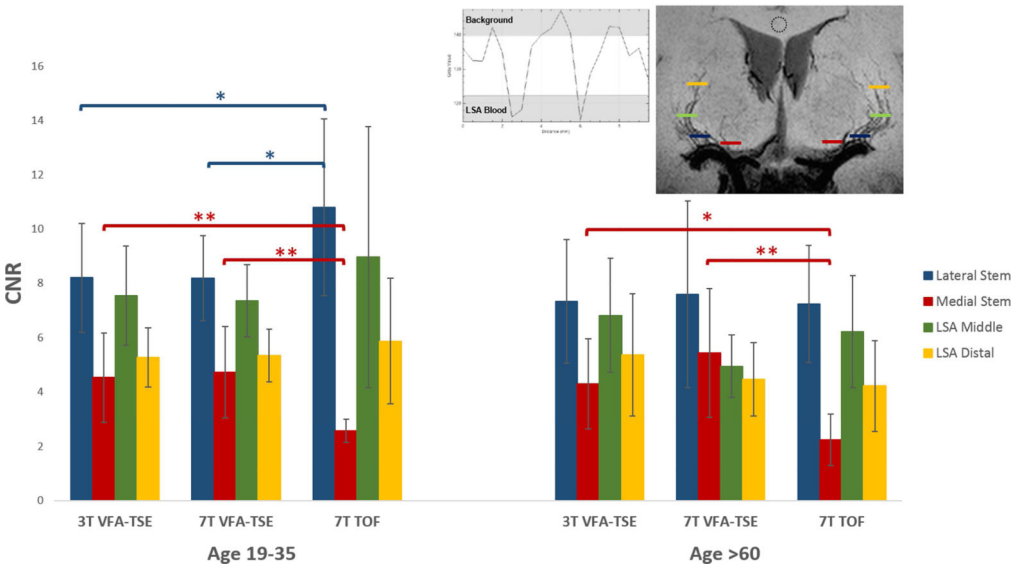

Figure 6.

CNR measures between blood and WM background in 3T VFA-TSE, 7T VFA-TSE, and 7T TOF images for different portions of the LSAs for age 19–35 years and age > 60 years respectively. The image intensity values were obtained by plotting the profiles across the regional planes (inset) and taking the mean of the top quartile as the tissue background signal and the mean of the bottom quartile of the signal plot profile as the vessel blood signal. Standard deviation of the noise was acquired from a region of interest (dotted circle) in tissue with relatively uniform contrast. * indicates significance ($p < 0.05$), ** indicates significance ($p \leq 0.001$).

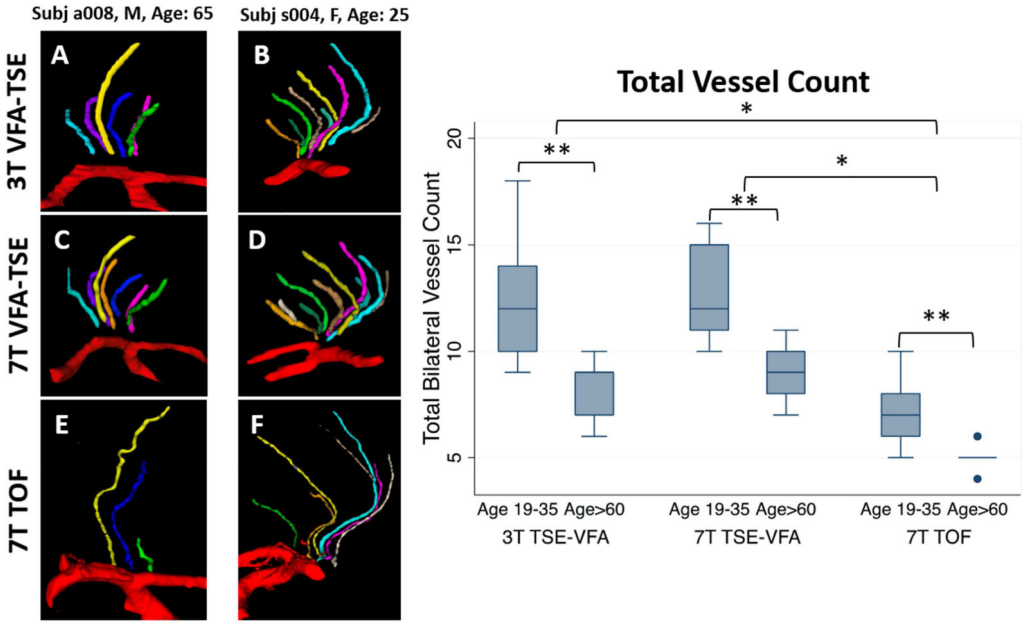

Figure 7.

Three-dimensional renderings of left LSAs from the manual segmentations of an aged subject (A,C,E) and a young subject (B,D,F). VFA-TSE at both 3T and 7T enabled the identification of more vessels in aged subjects, especially in the medial region. 7T VFA-TSE enabled the identification of more branches in general in the younger subjects (i.e. orange and turquoise branch vessels in D). Despite longer segmentation of vessels using 7T TOF images, fewer vessels could be identified. As summarized by the box plot of vessel count, significantly more vessels were detected in young subjects than in aged subjects (**, $p<0.01$), and more vessels were detected using VFA-TSE compared to 7T TOF MRA (*, $p<0.05$).

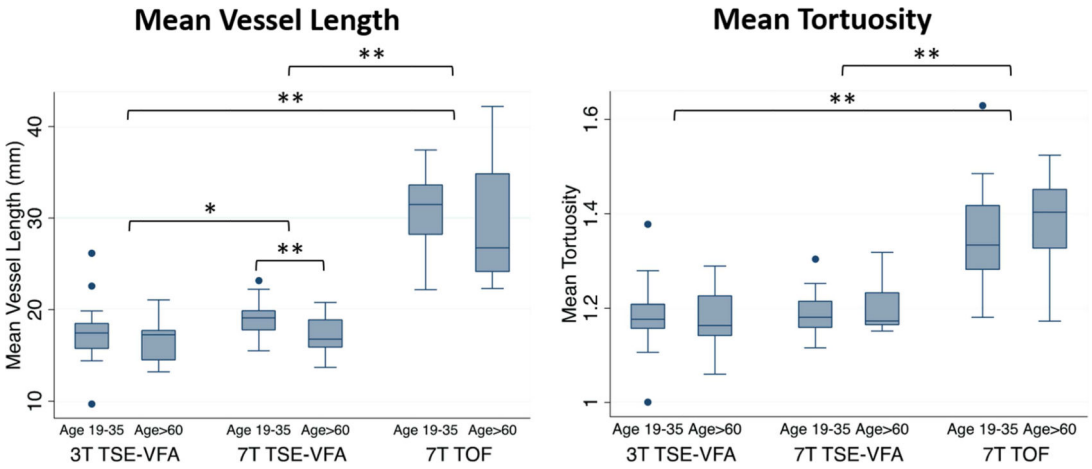

Figure 8.

Comparison of mean vessel length and tortuosity of lenticulostriate arteries in young (age 19–35 years) and aged (age > 60 years) groups for each modality. * indicates significance $p<0.05$; ** indicates significance $p<0.01$.

Table 1.

Summary of imaging parameters for sequences used in this study

	3T T1w VFA TSE	7T T1w VFA TSE	7T TOF MRA
Bandwidth (Hz/pixel)	360	504	120
Resolution (mm^3)	0.51 × 0.51 × 0.64	0.5 × 0.5 × 0.5	0.3 × 0.3 × 0.3
TE/TR (ms)	12/1000	13/1200	4.67/12.0
Orientation	Sagittal	Sagittal	Axial
FOV Read	230	160	200
FOV Phase	194	160	163
Turbo Factor	44	40	--
Echo Train Duration (ms)	162	175	--
Slices	160	288	72
Slice Oversampling	1.1	1	1.33
Y Partial Fourier	0.61	Off	7/8
Z Partial Fourier	0.78	5/8	7/8
Accel. Factor PE	2	3	3
Echo Spacing (ms)	5.78	4.08	--
Acquisition Time	8:39	10:05	9:25

Table 2.

Summary of Reeb graph metrics for 3T and 7T VFA-TSE manual segmentations of young and aged subjects (mean ± SD)

Metric	3T VFA-TSE		7T VFA-TSE		7T TOF	
	>60 years old	<35 years old	>60 years old	<35 years old	>60 years old	<35 years old
Total Bilateral Count	8.20 ± 1.64	12.17 ± 2.69	9.00 ± 1.58	12.75 ± 2.01	5.00 ± 0.71	7.20 ± 1.55
Vessel Length (mm)	16.62 ± 2.41	17.38 ± 3.11	17.06 ± 2.09	18.93 ± 1.99	28.92 ± 6.59	30.78 ± 4.70
Tortuosity	1.17 ± 0.07	1.18 ± 0.07	1.20 ± 0.05	1.19 ± 0.04	1.39 ± 0.11	1.35 ± 0.10